EES Batteries

ROYAL SOCIETY OF CHEMISTRY

COMMUNICATION

View Article Online
View Journal | View Issue



Cite this: *EES Batteries*, 2025, **1**, 808

Received 13th April 2025,
Accepted 2nd May 2025

DOI: 10.1039/d5eb00068h

rsc.li/EESBatteries

# Reverse Ragone *vs.* Direct Ragone plots: a comparative study for ultra-fast charging lithium-ion batteries

Shiqi Li [a,b] and Rachid Yazami *[b]

**A new concept of "Reverse" Ragone plots (RevRg) is introduced as opposed to the well-known "Direct" Ragone plots (DirRg). RevRg typically addresses the question of how much energy a lithium-ion battery (LIB) delivers according to the charging time. In contrast, DirRg predicts the amount of energy a LIB delivers from the initial full charge state according to the discharging time. In both RevRg and DirRg tests, the energy during discharge converts to the energy density $E_d$ (W h kg$^{-1}$), whereas the charging and discharging times convert to the power densities $\tilde{P}_c$ and $\tilde{P}_d$ (W kg$^{-1}$), leading to the RevRg and DirRg plots. The constant current-constant voltage (CCCV) charging method and a newly developed non-linear voltammetry (NLV) charging method are used for RevRg and DirRg tests on LIB cells. It is found that the NLV method occasionally enables full charging as fast as in 10 minutes, achieving much higher $E_d$ than CCCV does in the same charging time.**

### Broader context

Current Ragone plots address the energy output of a storage system such as batteries according to the utilisation (discharge) power. Our new concept of "Reverse Ragone" addresses the question of how much energy can be stored according to the charging time, which is more relevant for the end user, especially in electric vehicle applications. We found that the newly developed non-linear voltammetry charging technology (NLV) allows much higher energy output than the conventional constant-current based technologies (CC) under a limited charging time. We tested three different commercially available lithium-ion cells designed one for high power, the other for mid-power/energy and the last one for high energy performances with NLV and CC charging under the same charging time set between 60 minutes and 10 minutes. For the three cells, the energy output under NLV charge is significantly higher than that in the CC charge whatever is the charging time. Accordingly, our argument is that NLV will gradually replace the conventional CC-based charging technology, especially in battery application areas where the charging time is critical such as in electric vehicles and power tools to cite a few.

## 1 Introduction

Since the introduction of energy–power (*E*–*P*) Ragone plots (DirRg) by D. V. Ragone in 1968,[1,2] the concept has been extensively used for energy storage system performance assessment, including batteries,[3–10] heat energy storage systems,[3,6,11] and supercapacitors.[6–10,12] Both theoretical[3,8,9,13–16] and applied science aspects[5,6,17–19] of the DirRg concept were considered in the previous studies.

One of the practical findings from DirRg when applied to electric mobility is predicting the driving range basically from a fully charged battery pack (energy) according to the average driving speed (discharge power). The Reverse Ragone (RevRg) concept, however, addresses a different question of what the driving range of an electric vehicle (EV) would be according to the charging time. The charging time is becoming a critical parameter especially in EV applications.[20] When a constant current (CC) based charging method such as constant current-constant voltage (CCCV) and multi-stage CC (MSCC) is used to reduce the charging time, higher currents should be applied.[13,21] This may cause overheating, premature termination of charging before reaching the target state-of-charge (SOC), risks of thermal events, and reduced battery lifespan.[20]

In this work, a new charging protocol based on non-linear voltammetry (NLV) enabling safe ultra-fast charging is used.[22,23] NLV differs from CC-based charging methods in that no CC is applied at any time. Instead, a series of short constant voltage (CV) steps are applied, separated with very short rest periods while monitoring the current response and temperature. A transition from one CV plateau to the next occurs according to the current response. DirRg and RevRg plots are

[a]*Department of Electrical and Computer Engineering, National University of Singapore, Singapore 117583*
[b]*KVI PTE LTD, Singapore 637144. E-mail: rachid@kvi-battery.com*

used here to account for LIB performance under NLV and CCCV charging methods. Our tests on three different lithium-ion cells clearly showed that NLV charging outperforms CC-based charging especially when the charging time falls below 20 minutes. NLV charging should become the preferred technology especially in electric vehicle applications where the charging time is crucial.

# 2 Experimental

Three cylindrical LIB cells manufactured by Samsung SDI Co., Ltd, namely 30T, 40T, and 50E cells, were used in this study. The cells feature a nominal voltage of 3.6 V and the same 21 700 cylindrical form factor, with rated capacities of 3 A h, 4 A h, and 4.9 A h for the 30T, 40T, and 50E cells, respectively. The 30T cell is a high-power cell and the 50E cell is a high-energy cell, while the 40T cell lies between the two. For each cell type, three samples were tested, two for the RevRg tests under NLV and CCCV charging and the third one for the classic Ragone test under various discharge C-rates. For clarity, the cells for the RevRg test under NLV charging are labeled as 30T-1, 40T-1, and 50E-1, the cells for the RevRg test under CCCV charging are labeled as 30T-2, 40T-2, and 50E-2, and the cells for the DirRg test are labeled as 30T-3, 40T-3, and 50E-3.

The cells were tested at a constant ambient temperature of 25 °C regulated by a thermal chamber ESPEC SU-642. Two thermocouples were attached to the surface near the positive end (PE) and negative end (NE) of the cells to monitor the surface temperatures. The temperature data were logged using a Measurement Computing USB-2408 data acquisition device. A temperature safety limit of 55 °C was set during the tests. The cells were cycled using an ITECH IT-M3902C bi-directional power supply, with voltage and current upper limits of 32 V and 80 A, respectively.

All fresh cells were firstly subjected to a CCCV cycle to assess the nominal capacity. The CCCV cycle begins with CC charging at 0.5 C-rate until the cell voltage reaches 4.2 V, followed by CV charging at 4.2 V until the current drops below the cutoff current of 0.05 C-rate. After charging, the cells rest for 30 minutes before being discharged at a constant current of 0.5 C-rate to the cutoff voltage of 2.6 V. The C-rate is a measure of the constant current relative to the cell's nominal capacity, with 1 C-rate representing a current that charges or discharges the cell in one hour. Specifically, 1 C-rate corresponds to a constant current of 3 A, 4 A, and 4.9 A for the 30T, 40T, and 50E cells.

### 2.1 RevRg test under NLV charging

A series of NLV charging tests were applied to the 30T-1, 40T-1, and 50E-1 cells. The NLV charging tests were set for target charging times of 60, 50, 40, 30, 20, and 15 minutes. The 30T-1 and 40T-1 cells underwent an additional NLV charging test with a 10-minute target charging time, as they can withstand higher current levels based on the datasheets. The cells were allowed to rest for 30 minutes before being discharged at 0.5 C-rate regardless of the target charging time. Since the cells have the same voltage window based on the datasheets, identical end conditions were set to determine the end of the NLV charging process.

### 2.2 RevRg test under CCCV charging

A series of CCCV charging tests were applied to the 30T-2, 40T-2, and 50E-2 cells. The CV level was set at 4.2 V for all CCCV tests. The CC rates were set at 1, 1.2, 1.5, 2, 3, and 4 C, which theoretically correspond to the charging times of 60, 50, 40, 30, 20, and 15 minutes. The 30T-2 and 40T-2 cells underwent an additional CCCV charging test with a CC rate of 6 C, corresponding to a 10-minute charging time. This was conducted to compare the performance of CCCV and NLV charging in the same charging time. The settings for the rest period and the discharging process were identical to those in the NLV charging tests.

### 2.3 DirRg test under various discharge C-rates

Initially, the 30T-3, 40T-3, and 50E-3 cells underwent full charge under 0.5 C to 4.2 V; then 4.2 V was applied until the current dropped below 0.05 C. After 30-minute rest, the cells were discharged at C-rates of 0.5, 1, 2, 3, 4, and 5 C to 2.6 V. The 40T-3 cell underwent two additional CCCV cycles with discharge rates of 6 and 7 C. The 30T-3 cell underwent five more CCCV cycles with discharge rates of 6, 7, 8, 9, and 10 C.

# 3 Results and discussion

Since CCCV charging is widely used, its charging profiles are not disclosed here. Fig. 1(a)–(c) illustrate the current ($I$), voltage ($V$), and cell temperature ($T$) profiles during NLV charging in ~20 min for the 30T-1 cell. The cell temperature increased from about 25 °C to around 36 °C, which was below the temperature safety limit. Similar $I$, $V$, and $T$ profiles were achieved during all the NLV tests, which are not reported here to avoid redundancy. NLV was proposed by Yazami *et al.*[22,23] NLV consists of applying a series of short CV steps separated by a very short rest time with no current injection. During each CV step, the charging current drops nearly according to the Cottrell equation $i = k{\cdot}t^{-1/2}$. The current profile during the CV step translates the resilience of the cell to taking more charge. During the short rest period of about 2 s, the cell voltage drops to the "pseudo-open-circuit voltage" (p-OCV).[24] The rest time between two CV steps allows for anode and cathode depolarization, which is overall an endothermic process, therefore contributing to reducing the cell's temperature rise rate during NLV charging. The voltage transition from one CV plateau to the next takes place according to the current dropping rate. The completion of NLV charging takes place when one of the following three conditions is achieved: (1) the target final SOC, (2) the voltage upper limit, and (3) the temperature safety limit.

### 3.1 RevRg plot

The RevRg plot is obtained by depicting the energy density $E_d$ during the discharging process *versus* the average charge

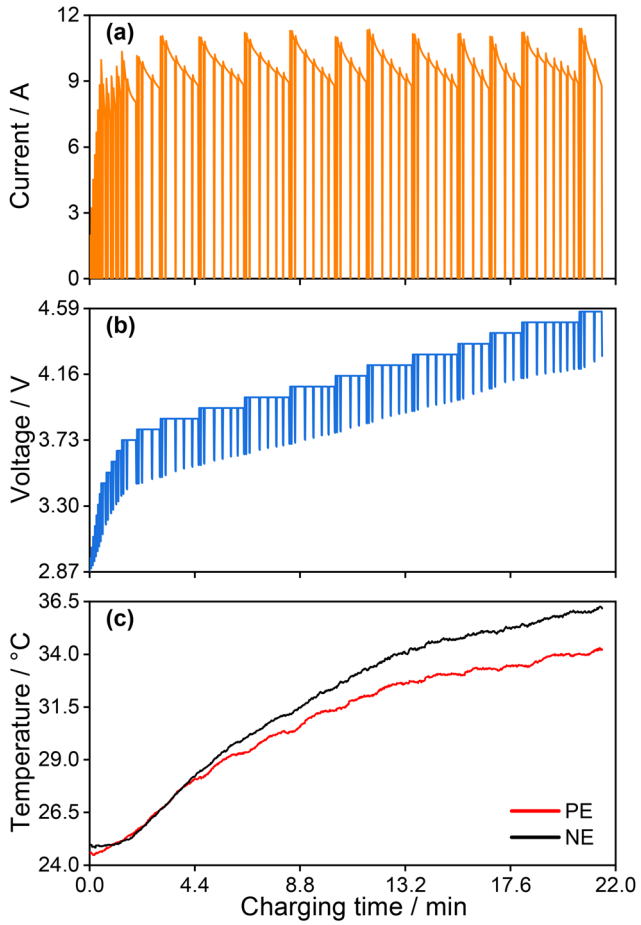


**Fig. 1** (a) Current, (b) voltage, and (c) cell temperature profiles during 20-minute NLV charging for the 30T-1 cell near the positive (PE) and negative electrode (NE).

power density $\bar{P}_c$. The following equations were used to calculate $E_d$ in W h kg$^{-1}$ and $\bar{P}_c$ in W kg$^{-1}$:

$$E_d = \frac{1}{M}\int_0^{t_d} V_d(t)\cdot I_d \mathrm{d}t \quad (1)$$

$$\bar{P}_c = \frac{1}{M\cdot t_c}\int_0^{t_c} V_c(t)\cdot I_c(t)\mathrm{d}t \quad (2)$$

where $M$ represents the mass of the cell, $V_d(t)$ is the voltage during the discharging process at a constant current of $I_d$, $V_c(t)$ and $I_c(t)$ indicate the voltage and current during the charging process, and $t_c$ and $t_d$ represent the total charging time and discharging time, respectively.

Fig. 2(a)–(c) show the RevRg plots for three types of cells under NLV (30T-1, 40T-1, and 50E-1) and CCCV (30T-2, 40T-2, and 50E-2) charging. The solid lines represent the RevRg curves under two charging protocols. The gray dashed lines are labeled with the target charging times in minutes. The highest energy density under 60-minute NLV charging is about 160 W h kg$^{-1}$, 210 W h kg$^{-1}$, and 247 W h kg$^{-1}$ for 30T, 40T, and 50E cells, respectively. However, when the charging time is decreased, 30T remarkably maintains a flat energy profile at

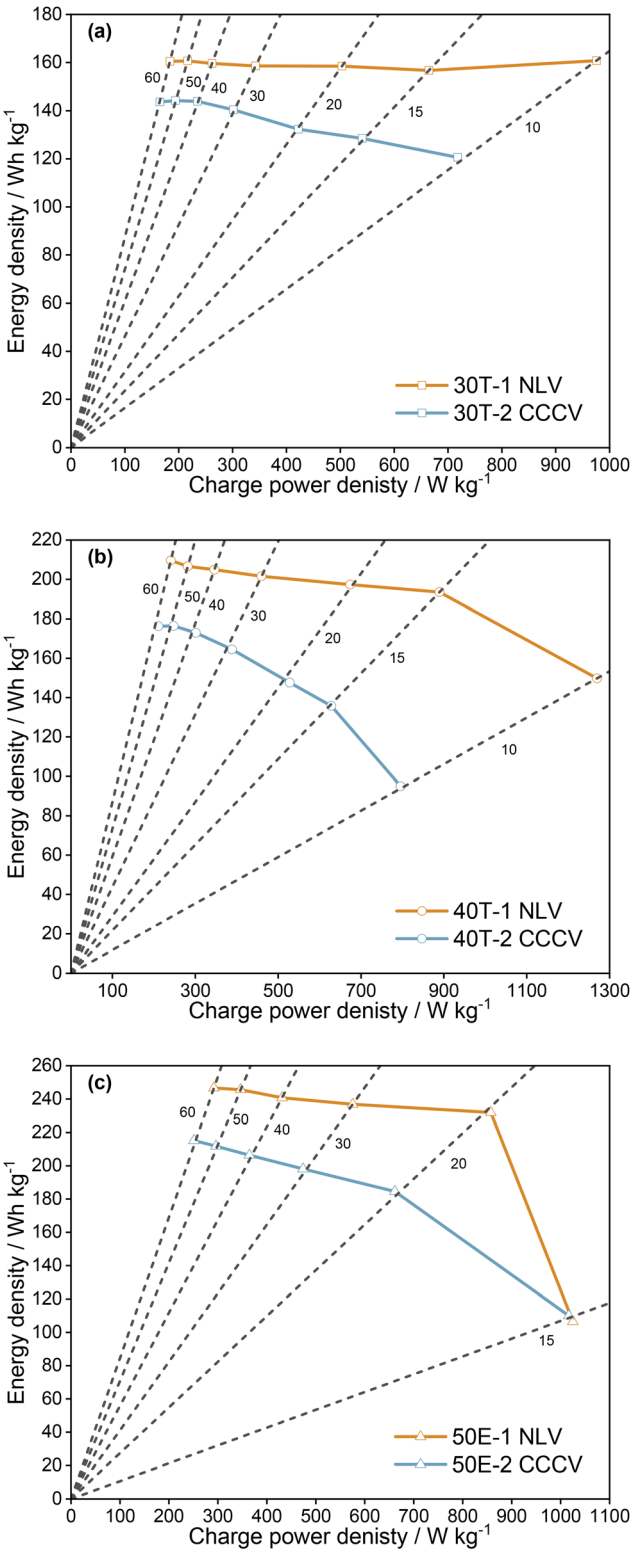


**Fig. 2** RevRg plots under NLV and CCCV charging for (a) 30T-1 and 30T-2, (b) 40T-1 and 40-2, and (c) 50E-1 and 50E-2 cells. The solid lines correspond to the RevRg plots, and the labels besides the gray dashed lines represent the charging times in minutes.

~160 W h kg$^{-1}$ even under 10-minute NLV charging. In contrast, the profiles for 40T and 50E show a negative slope, which becomes more pronounced for the charging time below 15 and 20 minutes for 40T and 50E cells, respectively. It is most worth noting that for the three cells, the discharge energy output is much higher under NLV charging than under CCCV charging in the same charging times. The only exception is the 50E cell in 15-minute charging time where the NLV and CCCV data are quite similar. The superiority of the NLV *vs.* CCCV charging protocol is obvious, since CCCV does not allow a full charge of the cell in limited times.

Furthermore, the RevRg plots provide insights into how to properly charge the cells in practical scenarios, ensuring they work under favorable charging conditions. For the 40T and 50E cells, although they show a higher energy density than the 30T cell, their sloping profile suggests a higher internal resistance, which impedes their ultra-fast charging performance. The highest cell temperatures achieved during NLV charging are 49 °C, 51 °C, and 55 °C for 30T in 10 minutes, 40T in 10 minutes, and 50E in 15 minutes, whereas the highest cell temperatures are 40 °C, 42 °C, and 46 °C during CCCV charging in the same times. The difference in temperature is probably due to the fact that NLV charging achieved much higher SOC than CCCV charging. It was observed that under higher charging rates, the temperature increases steadily in the ~80–100% SOC range due to the cell's overpotential.

### 3.2 DirRg plot

For DirRg tests, the energy density was obtained using eqn (1) and the average discharge power density was calculated using eqn (3)

$$\bar{P}_{\mathrm{d}} = \frac{1}{M \cdot t_{\mathrm{d}}} \int_0^{t_{\mathrm{d}}} V_{\mathrm{d}}(t) \cdot I_{\mathrm{d}}(t) \mathrm{d}t \quad (3)$$

Fig. 3 shows the DirRg plots for three fully charged cells under various discharge C-rates. The highest energy density under 0.5 C-rate discharge is about 160 W h kg$^{-1}$, 208 W h kg$^{-1}$, and 248 W h kg$^{-1}$ for 30T, 40T, and 50E cells, respectively. At higher discharge C-rates, the energy density of the three cells decreases at different slopes, since the cutoff voltage of 2.6 V can be reached before the cells are fully discharged. The slopes for 30T-3, 40T-3, and 50E-3 cells become more pronounced at a discharge C-rate higher than 6 C, 5 C, and 3 C, respectively. Performance limitations of the cells at a high-power region are attributed to the ohmic losses associated with higher polarization effects. The DirRg plots demonstrate that a demanding discharge pattern can result in less energy output. Moreover, the results demonstrate that the 30T and 40T cells are well-suited for high-power applications with discharge C-rates around 5 C, whereas the 50E cell is preferred in high-energy scenarios under non-intensive discharge patterns with C-rates below 3 C. It is noteworthy that the 30T cell outperforms the 40T and 50E cells above 1000 W h kg$^{-1}$ discharge power density, highlighting its high-power characteristics.

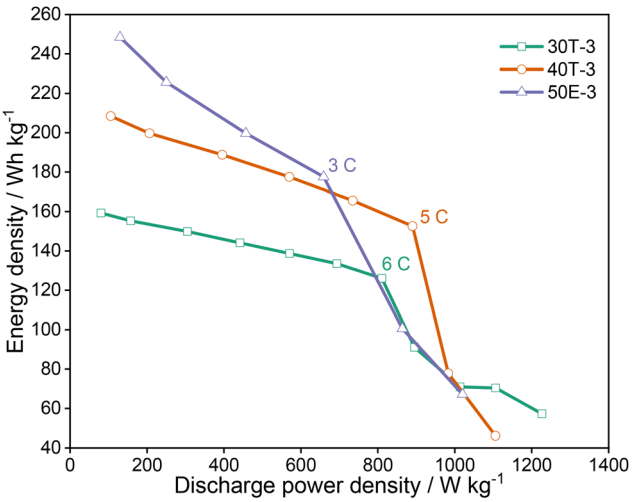


Fig. 3 DirRg plots for the three cells under various discharge C-rates. The slopes of DirRg curves exhibit changes when the discharge C-rate exceeds 6 C, 5 C, and 3 C for 30T-3, 40T-3, and 50E-3 cells.

## 4 Conclusion

In this work, the Reverse Ragone (RevRg) concept is introduced for the first time to account for the energy output of a LIB cell according to the charging time. RevRg provides particularly useful data in LIB applications where the charging time is critical such as in EVs and in power tools. It is found that the NLV ultra-fast charging method outperforms the conventional CCCV charging method on the charging time basis. Under NLV charging, the high-power density 30T cell showed a nearly constant discharge energy density over a charging time range of 10 to 60 minutes, whereas the energy density declined steadily with shorter charging times under CCCV charging. The 40T and 50E cells, however, showed a declining energy density under both NLV and CCCV charging, although the declining slope is larger under the CCCV charging protocol. The 40T cell showed the best tradeoff between energy and power even under 10-minute NLV charging. Owing to its adaptive charging characteristics, NLV outperforms CCCV charging and is anticipated to gradually become a preferred charging method of LIB-based systems, particularly in the electric mobility space.

## Data availability

All data in the manuscript referred to above are original data generated from battery testing in our laboratories. They have never been published elsewhere, nor have they been presented at a public event. Data are being made available only for the purpose of publication in *EES Batteries*.

The data supporting this article have been included as part of the manuscript.

## Conflicts of interest

There are no conflicts to declare.

## References

1 D. V. Ragone, *Mater. Eng.*, 1968, **68**, 34–36.
2 D. V. Ragone, *SAE Technical Paper* 680453, 1968.
3 T. Christen, *J. Energy Storage*, 2020, **27**, 101084.
4 I. S. Sarpal, A. Bensmann, J. Mähliß, D. Hennefeld and R. Hanke-Rauschenbach, *Int. J. Electr. Power Energy Syst.*, 2018, **99**, 722–732.
5 Y. Chen, E. Macii and M. Poncino, 2016 IFIP/IEEE International Conference on Very Large Scale Integration (VLSI-SoC), 2016, pp. 1–6.
6 I. Beyers, A. Bensmann and R. Hanke-Rauschenbach, *J. Energy Storage*, 2023, **73**, 109097.
7 B. D. McCloskey, *J. Phys. Chem. Lett.*, 2015, **6**, 3592–3593.
8 W. Pell and B. Conway, *J. Power Sources*, 1996, **63**, 255–266.
9 D. Cericola, P. W. Ruch, R. Kötz, P. Novák and A. Wokaun, *J. Power Sources*, 2010, **195**, 2731–2736.
10 Y. C. Zhang, O. Briat, L. Boulon, J.-Y. Deletage, C. Martin, F. Coccetti and J.-M. Vinassa, *Appl. Energy*, 2019, **247**, 703–715.
11 J. Woods, A. Mahvi, A. Goyal, E. Kozubal, A. Odukomaiya and R. Jackson, *Nat. Energy*, 2021, **6**, 295–302.
12 Y. W. Foong and K. H. Bevan, *J. Phys.: Energy*, 2024, **6**, 015019.
13 T. Christen and M. W. Carlen, *J. Power Sources*, 2000, **91**, 210–216.
14 E. M. Krieger and C. B. Arnold, *J. Power Sources*, 2012, **210**, 286–291.
15 T. Christen and C. Ohler, *J. Power Sources*, 2002, **110**, 107–116.
16 E. Catenaro, D. M. Rizzo and S. Onori, *Appl. Energy*, 2021, **291**, 116473.
17 C. F. de Freitas, P. Bartholomeus, X. Margueron and P. Le Moigne, 2021 IEEE Vehicle Power and Propulsion Conference (VPPC), 2021, pp. 1–6.
18 A. Rufer, *Facta Univ., Series: Electron. Energ.*, 2024, **37**, 249–260.
19 S. K. Kumar, A. A. Abduh, O. Sabih and R. Yazami, *J. Electrochem. Soc.*, 2018, **165**, A674.
20 A. Tomaszewska, Z. Chu, X. Feng, S. O'kane, X. Liu, J. Chen, C. Ji, E. Endler, R. Li, L. Liu, *et al.*, *eTransportation*, 2019, **1**, 100011.
21 I. Goncharova and R. Yazami, *Int. J. Eng. Sci.*, 2019, **8**, 57–64.
22 R. Yazami and T. G. T. A. Bandara, *U. S. patent application*, 202116721, 2021.
23 T. A. Bandara and R. Yazami, *Int. J. Eng. Sci.*, 2018, **7**, 44–58.
24 S. Li, J. C.-H. Peng and R. Yazami, *J. Power Sources*, 2024, **624**, 235595.